Inorg. Chem. **2003**, *42*, 2842–2848

Monolayer, Bilayer, Multilayers: Evolving Magnetic Behavior in Langmuir–Blodgett Films Containing a Two-Dimensional Iron–Nickel Cyanide Square Grid Network

Jeffrey T. Culp,[†] Ju-Hyun Park,[‡] Mark W. Meisel,*[,‡] and Daniel R. Talham*[,†]

Department of Chemistry, University of Florida, Gainesville, Florida 32611-7200, and Department of Physics and Center for Condensed Matter Sciences, University of Florida, Gainesville, Florida 32611-8440

Received November 6, 2002

The assembly of two-dimensional cyanide-bridged Fe^{III}–Ni^{II} square grid networks at the air–water interface and subsequent transfer of these networks as isolated monolayer, isolated bilayer, and multiple bilayer (multilayer) films via the Langmuir–Blodgett technique results in novel low-dimensional systems in which the effects of dimensionality on magnetic behavior in molecule-based materials can be observed. The magnetic response of these films between $2 < T < 300$ K in dc fields from $-50 < H < 50$ kG and in 4 G ac fields from 1 Hz to 1 kHz are reported. The results show the presence of ferromagnetic domains with characteristic hysteresis in each of the three systems. The magnetic response for all three samples is anisotropic with a stronger field-cooled magnetization observed when the planes of the films are aligned parallel to the applied field. Additionally, each of the three samples shows frequency dependence in both the real and imaginary components of the ac susceptibility. This behavior is interpreted as being characteristic of spin glass-type ordering of ferromagnetic domains to form a cluster glass. A lower glass temperature (T_g) is observed in the isolated monolayer film relative to the bilayer and multilayer samples. The bilayer sample shows two glass transitions at $T_{g1} = 3.8$ K and $T_{g2} = 5.4$ K, whereas only one transition at $T_g = 5.4$ K is observed in the multilayer sample. The different magnetic responses of the three films are attributed to different in-plane, interplane, and long-range dipolar exchange interactions.

Introduction

Solid-state metal cyanides are a structurally diverse class of materials. The best known examples come from the family of "Prussian blues" (named after the deep blue mixed-valency $Fe^{III}[Fe^{II}(CN)_6]$) which consist of octahedral $[M(CN)_6]^{n-}$ complexes bridged through metal ions to form three-dimensional cubic solids.[1] However, many other structural motifs have also been realized by introducing "blocking ligands" to one or both of the metal complex building blocks, thereby lowering the symmetry of the final cyanide-bridged arrays. This strategy has yielded a variety of structures over a wide range of dimensionality including clusters,[2−9] molecular squares,[10,11] linear chains,[12−14] and ladders[15,16] as well as quasi-two-dimensional square-grid[17−20] and "honeycomb" networks.[21−25]

Aside from their structural diversity, metal cyanides also show interesting magnetic behavior. For many examples, the nature of the magnetic exchange can be anticipated in

* To whom correspondence should be addressed. E-mail: talham@chem.ufl.edu (D.R.T.).
[†] Department of Chemistry.
[‡] Department of Physics and Center for Condensed Matter Sciences.

(1) Buser, H. J.; Schwarzenbach, D.; Petter, W.; Ludi, A. *Inorg. Chem.* **1977**, *16*, 2704−2710.
(2) Shores, M. P.; Sokol, J. J.; Long, J. R. *J. Am. Chem. Soc.* **2002**, *124*, 2279−2292.
(3) Berseth, P. A.; Sokol, J. J.; Shores, M. P.; Heinrich, J. L.; Long, J. R. *J. Am. Chem. Soc.* **2000**, *122*, 9655−9662.
(4) Heinrich, J. L.; Sokol, J. J.; Hee, A. G.; Long, J. R. *J. Solid State Chem.* **2001**, *159*, 293−301.
(5) Larionova, J.; Gross, M.; Pilkington, M.; Andres, H.; Stoeckli-Evans, H.; Gudel, H. U.; Decurtins, S. *Angew. Chem., Int. Ed.* **2000**, *39*, 1605−1609.
(6) Rogez, G.; Parsons, S.; Paulsen, C.; Villar, V.; Mallah, T. *Inorg. Chem.* **2001**, *40*, 3836−3837.
(7) Parker, R. J.; Spiccia, L.; Berry, K. J.; Fallon, G. D.; Moubaraki, B.; Murray, K. S. *Chem. Commun.* **2001**, 333−334.
(8) Scuiller, A.; Mallah, T.; Verdaguer, M.; Nivorozkhin, A.; Tholence, J. L.; Veillet, P. *New J. Chem.* **1996**, *20*, 1−3.
(9) Mallah, T.; Auberger, C.; Verdaguer, M.; Veillet, P. *Chem. Commun.* **1995**, 61−62.
(10) Oshio, H.; Onodera, H.; Tamada, O.; Mizutani, H.; Hikichi, T.; Ito, T. *Chem.—Eur. J.* **2000**, *6*, 2523−2530.

10.1021/ic026158x CCC: $25.00
Published on Web 03/27/2003

Scheme 1. Assembly of Langmuir−Blodgett Films Containing an Iron−Nickel Cyanide Square Grid Network

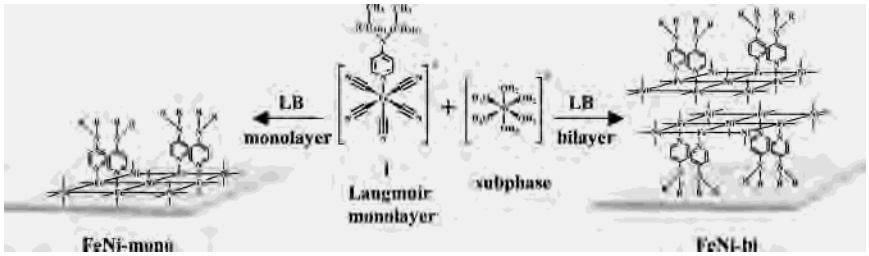

advance from basic orbital interaction arguments and the predictable structure-directing quality of the cyanide bridge.[26] This inherent ability to tailor both the structure and magnetic exchange in metal cyanide systems makes this family of materials well suited for studying molecule-based magnetic phenomena. Indeed, a wide range of magnetic phenomena have been observed in metal cyanides, including high-spin clusters,[2−9] metamagnetism,[19,23,25,27−30] room-temperature magnetic ordering,[31−34] and spin-glass behavior.[35,36]

We have recently described the synthesis of a cyanide-bridged $Fe^{III}-Ni^{II}$ square grid network as a monolayer at the air−water interface and its transfer to solid supports by the Langmuir−Blodgett (LB) technique.[37] This two-dimensional (2D) network can be transferred as an isolated monolayer, as a single bilayer, or as multiple-bilayer assemblies (see Scheme 1). Initial magnetic property investigations of multilayer films (multiple-bilayer films) by dc magnetometry revealed ferromagnetism below 8 K.

Single-layer control over the deposition process provides an opportunity to observe how the magnetic properties of the system evolve as it changes from a monolayer to a bilayer to a multilayer film. We report herein a detailed investigation of the magnetic properties of this 2D system using both dc and ac magnetometry which reveals both ferromagnetic and spin-glass-like behavior at low temperatures.

Experimental Details

Materials. Nickel nitrate hexahydrate (99%) was purchased from Aldrich (Milwaukee, WI) and used as received. The amphiphilic complex **1** [bis(tetramethylammonioum) pentacyano(4-(didodecylamino)pyridine)ferrate(III)·$6H_2O$] was prepared as described.[37] Subphase solutions were prepared from 17.8−18.1 MΩ cm water delivered with a Barnstead Epure system.

Film Preparation. All films were prepared on Mylar substrates precleaned with absolute ethanol. The 150 bilayer/side sample was prepared as previously described.[37] Briefly, a Langmuir monolayer of complex **1** is reacted at the air−water interface over a subphase containing 1 g/L of $Ni(NO_3)_2·6H_2O$ (see Scheme 1). The resulting square grid network that forms is transferred at a surface pressure of 25 mN/m as a Y-type film by the Langmuir−Blodgett technique. The transfer ratio (T_R) of the 150 bilayer sample (**FeNi-150**) was $T_R = 1.0 \pm 0.1$ for both the upstrokes and downstrokes throughout the transfer process (where $T_R = 1.0$ signifies a complete monolayer transfer). A separate sample consisting of a single bilayer (**FeNi-bi**), i.e., one downstroke followed by one upstroke, was prepared on a Mylar surface precoated with 5 bilayers of octadecanol for increased hydrophobicity. The transfer ratios for **FeNi-bi** were $T_R = 1.0 \pm 0.1$ for both the downstroke and upstroke. A sample consisting of a single monolayer of the Fe−Ni grid network (**FeNi-mono**) was prepared using a single transfer starting with the Mylar

(11) Oshio, H.; Tamada, O.; Onodera, H.; Ito, T.; Ikoma, T.; Tero-Kubota, S. *Inorg. Chem.* **1999**, *38*, 5686−5689.
(12) Kou, H. Z.; Liao, D. Z.; Jiang, Z. H.; Yan, S. P.; Wu, Q. J.; Gao, S.; Wang, G. L. *Inorg. Chem. Commun.* **2000**, *3*, 151−154.
(13) Ohba, M.; Usuki, N.; Fukita, N.; Okawa, H. *Inorg. Chem.* **1998**, *37*, 3349−3354.
(14) Cernak, J.; Orendac, M.; Potocnak, I.; Chomic, J.; Orendacova, A.; Skorsepa, J.; Feher, A. *Coord. Chem. Rev.* **2002**, *224*, 51−66.
(15) Ohba, M.; Fukita, N.; Okawa, H. *J. Chem. Soc., Dalton Trans.* **1997**, 1733−1737.
(16) Ohba, M.; Maruono, N.; Okawa, H.; Enoki, T.; Latour, J. M. *J. Am. Chem. Soc.* **1994**, *116*, 11566−11567.
(17) Ohba, M.; Okawa, H.; Ito, T.; Ohto, A. *Chem. Commun.* **1995**, 1545−1546.
(18) Ohba, M.; Okawa, H.; Fukita, N.; Hashimoto, Y. *J. Am. Chem. Soc.* **1997**, *119*, 1011−1019.
(19) Kou, H. Z.; Tang, J. K.; Liao, D. Z.; Gao, S.; Cheng, P.; Jiang, Z. H.; Yan, S. P.; Wang, G. L.; Chansou, B.; Tuchagues, J. P. *Inorg. Chem.* **2001**, *40*, 4839−4844.
(20) Kou, H. Z.; Bu, W. M.; Liao, D. Z.; Jiang, Z. H.; Yan, S. P.; Fan, Y. G.; Wang, G. L. *J. Chem. Soc., Dalton Trans.* **1998**, 4161−4164.
(21) Colacio, E.; Dominguez-Vera, J. M.; Ghazi, M.; Kivekas, R.; Lloret, F.; Moreno, J. M.; Stoeckli-Evans, H. *Chem. Commun.* **1999**, 987−988.
(22) Ferlay, S.; Mallah, T.; Vaissermann, J.; Bartolome, F.; Veillet, P.; Verdaguer, M. *Chem. Commun.* **1996**, 2481−2482.
(23) Kou, H. Z.; Gao, S.; Bu, W. M.; Liao, D. Z.; Ma, B. Q.; Jiang, Z. H.; Yan, S. P.; Fan, Y. G.; Wang, G. L. *J. Chem. Soc., Dalton Trans.* **1999**, 2477−2480.
(24) Kou, H. Z.; Bu, W. M.; Gao, S.; Liao, D. Z.; Jiang, Z. H.; Yan, S. P.; Fan, Y. G.; Wang, G. L. *J. Chem. Soc., Dalton Trans.* **2000**, 2996−3000.
(25) Kou, H. Z.; Gao, S.; Bai, O.; Wang, Z. M. *Inorg. Chem.* **2001**, *40*, 6287−6294.
(26) Verdaguer, M.; Bleuzen, A.; Marvaud, V.; Vaissermann, J.; Seuleiman, M.; Desplanches, C.; Scuiller, A.; Train, C.; Garde, R.; Gelly, G.; Lomenech, C.; Rosenman, I.; Veillet, P.; Cartier, C.; Villain, F. *Coord. Chem. Rev.* **1999**, *192*, 1023−1047.
(27) Kou, H. Z.; Gao, S.; Ma, B. Q.; Liao, D. Z. *Chem. Commun.* **2000**, 1309−1310.
(28) Marvilliers, A.; Parsons, S.; Riviere, E.; Audiere, J. P.; Kurmoo, M.; Mallah, T. *Eur. J. Inorg. Chem.* **2001**, 1287−1293.
(29) Re, N.; Crescenzi, R.; Floriani, C.; Miyasaka, H.; Matsumoto, N. *Inorg. Chem.* **1998**, *37*, 2717−2722.
(30) Ohba, M.; Okawa, H. *Coord. Chem. Rev.* **2000**, *198*, 313−328.
(31) Holmes, S. M.; Girolami, G. S. *J. Am. Chem. Soc.* **1999**, *121*, 5593−5594.
(32) Hatlevik, O.; Buschmann, W. E.; Zhang, J.; Manson, J. L.; Miller, J. S. *Adv. Mater.* **1999**, *11*, 914−918.
(33) Ferlay, S.; Mallah, T.; Ouahes, R.; Veillet, P.; Verdaguer, M. *Nature* **1995**, *378*, 701−703.
(34) Dujardin, E.; Ferlay, S.; Phan, X.; Desplanches, C.; Moulin, C. C. D.; Sainctavit, P.; Baudelet, F.; Dartyge, E.; Veillet, P.; Verdaguer, M. *J. Am. Chem. Soc.* **1998**, *120*, 11347−11352.
(35) Buschmann, W. E.; Ensling, J.; Gutlich, P.; Miller, J. S. *Chem.—Eur. J.* **1999**, *5*, 3019−3028.
(36) Buschmann, W. E.; Miller, J. S. *Inorg. Chem.* **2000**, *39*, 2411−2421.
(37) Culp, J. T.; Park, J.-H.; Stratakis, D.; Meisel, M. W.; Talham, D. R. *J. Am. Chem. Soc.* **2002**, *124*, 10083−10090.

immersed in the subphase, i.e., hydrophilic transfer. The transfer ratio for **FeNi-mono** was $T_R = 1.0 \pm 0.1$.

For magnetic measurements, each 10 cm^2 sample was cut and packed into gel caps for SQUID magnetometry. The rectangular pieces were packed parallel to one another and orientated with the plane of the sample surface aligned parallel (∥) or perpendicular (⊥) to the applied dc or ac magnetic fields. Background corrections were applied by subtraction of the diamagnetic signal measured on a similar (within 3%) mass of clean Mylar and sample container ($\chi_{dia} = -2.16 \times 10^{-7}$ emu).

Instrumentation. The LB films were prepared by using a KSV Instruments 5000 trough modified to operate with double barriers. The surface pressure was measured with a filter paper Wilhelmy plate suspended from a KSV microbalance. Magnetization measurements were performed on a Quantum Design MPMS SQUID magnetometer. For the ac susceptibility, χ_{AC}, all measurements of the in-phase (real or dispersive) susceptibility, χ', and out-of-phase (imaginary or absorptive) susceptibility, χ'', were made after zero-field-cooling the sample, with subsequent warming under zero-applied dc field and an oscillating ac field of 4 G.

Results

The two-dimensional grid network, prepared as shown in Scheme 1, has been structurally characterized by grazing incidence X-ray diffraction, X-ray absorption fine structure, infrared spectroscopy, and X-ray photoelectron spectroscopy.[37] The in-plane structure of the network consists of a face-centered square grid of low-spin Fe^{III} ions which are bridged through cyanide to Ni^{II} ions. The in-plane lattice parameter is $a = 10.4$ Å, which yields an Fe−Ni separation of 5.2 Å. The average structural coherence length, as determined from X-ray diffraction, is approximately 6 unit cell lengths. This value gives an average coherent particle size on the order of 3600 Å^2, which would contain approximately 144 ions (72 Fe^{III} ions and 72 Ni^{II} ions).

As depicted in Scheme 1, the networks can be transferred to solid supports in a controlled fashion by the LB technique. If the dipping cycle begins with the substrate submerged, withdrawing the substrate results in the transfer of a single monolayer of the Fe−CN−Ni network (**FeNi-mono**) oriented such that the inorganic network is in direct contact with the substrate surface. In this case, the planar network is an isolated two-dimensional system (it is not truly isolated, as an anisotropic background arises from the substrate). On the other hand, if the substrate begins above the water surface, one dipping cycle of passing the substrate into the subphase and back out results in a bilayer (**FeNi-bi**), with the organic portion of the material in contact with the substrate and the inorganic networks face-to-face, sandwiched in the center of the bilayer. The nature of the bonding interaction in the polar region between the networks is uncertain but likely contains a mixture of covalent bonding via coordination of the axial cyanide of the iron complex to Ni^{2+} ions in the adjacent layer, hydrogen bonding via intercalated water molecules, or simple electrostatic interactions. These interactions should give an average distance between inorganic networks within the bilayer on the order of 10 Å or less. Finally, if the dipping cycle is repeated though 150 cycles (**FeNi-150**), each bilayer of the Fe−CN−Ni network will be deposited onto the previous bilayer forming a Y-type LB film with alternating regions of organic-to-organic and inorganic-to-inorganic contacts.

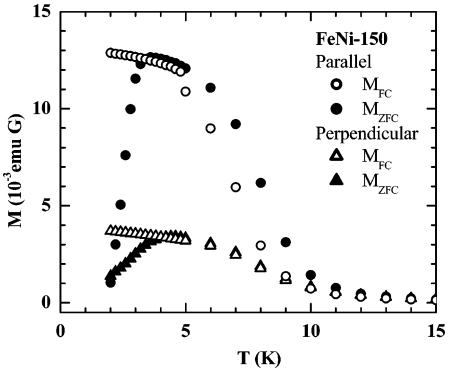

Figure 1. Background-corrected magnetization vs temperature for **FeNi-150** aligned parallel to the applied field [(○) field-cooled and (●) zero-field-cooled] and perpendicular to the applied field [(△) field-cooled and (▲) zero-field cooled]. Cooling fields and measuring fields were each 100 G.

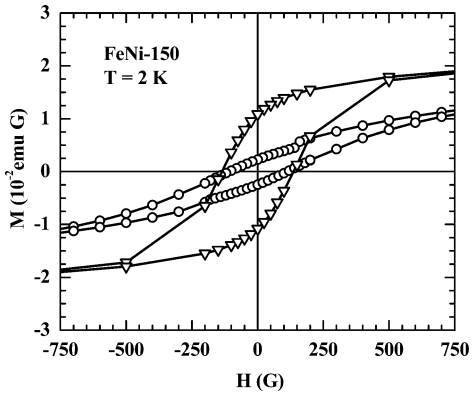

Figure 2. Background-corrected magnetization vs field measured at 2 K for **FeNi-150** aligned parallel (▽) to the applied field and perpendicular (○) to the applied field. (The total sweep width was −50 to 50 kG.) The lines are guides to the eye.

Dc Magnetometry. The field-cooled (M_{FC}) and zero-field-cooled (M_{ZFC}) magnetization plots as a function of temperature for **FeNi-150** in two orientations with respect to the applied field are shown in Figure 1. Both field-cooled curves show a rapid rise in magnetization at lower temperatures below approximately 10 K, gradually leveling below 5 K. This behavior is indicative of ferromagnetic exchange in the film. Ferromagnetism in this system is rationalized as resulting from low-spin $S = 1/2$ Fe^{III} t_{2g} and $S = 1$ Ni^{II} e_g magnetic orbitals overlapping with orthogonal orbitals on the cyanide bridge favoring the maximum total spin in accordance with Hund's rule. The field-cooled magnetic response of the film is clearly anisotropic, reflecting the planar anisotropy of the network.

Ferromagnetism in **FeNi-150** is also supported by hysteresis in M vs H at $T = 2$ K as shown in Figure 2. Again, the magnetization is anisotropic with a larger remnant magnetization when the sample is aligned parallel to the applied field. The coercive fields are slightly anisotropic as well with $H_c = 135 \pm 5$ G in the parallel orientation and $H_c = 110 \pm 5$ G in the perpendicular orientation. The nature of the LB film samples results in significant diamagnetic background

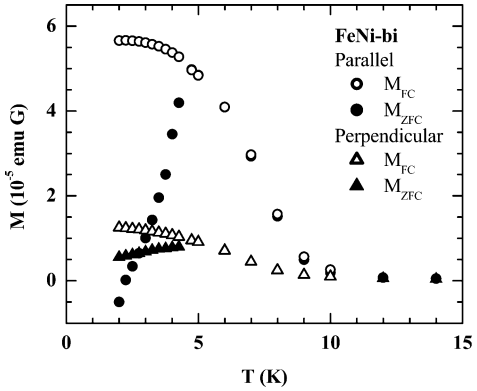

Figure 3. Background-corrected magnetization vs temperature for **FeNi-bi** aligned parallel and perpendicular to the applied field. Cooling fields and measuring fields were each 20 G.

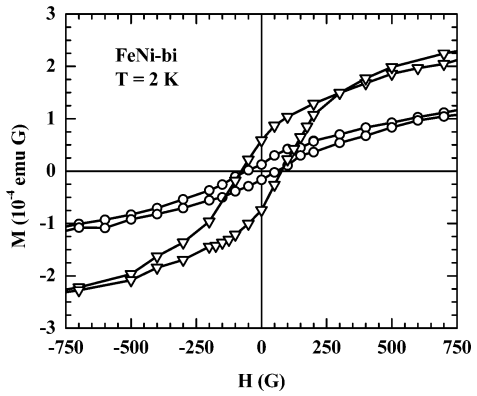

Figure 4. Background-corrected magnetization vs field measured at 2 K for **FeNi-bi** aligned parallel (▽) to the applied field and perpendicular (○) to the applied field. (The total sweep width was −50 to 50 kG.) The lines are guides to the eye.

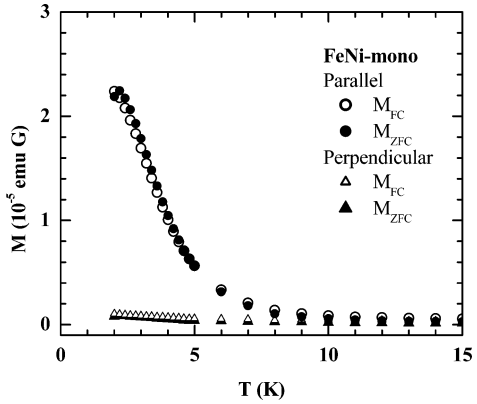

Figure 5. Background-corrected magnetization vs temperature for **FeNi-mono** aligned parallel and perpendicular to the applied field. Cooling fields and measuring fields were each 20 G.

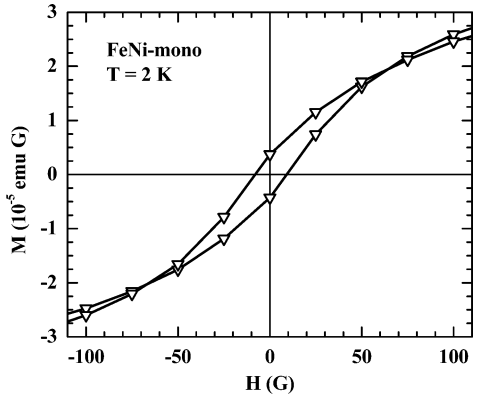

Figure 6. Background-corrected magnetization vs field measured at 2 K for **FeNi-mono** aligned parallel to the applied field. (The total sweep width was −50 to 50 kG.) The lines are guides to the eye.

arising from the substrate and sample container, making it difficult to quantify the film response at high magnetic fields. Therefore, the saturation moment and saturation fields are not well defined.

Plots of the magnetization of **FeNi-bi** as a function of temperature for both field-cooling and zero-field-cooling are shown in Figure 3. Data are shown for the parallel and perpendicular orientations. As observed in the multilayer sample, there is a sudden rise in the field-cooled magnetization below 10 K, signaling ferromagnetic exchange that again levels off below 4 K. The field-cooled magnetic response shows a slightly larger anisotropy than observed in the multilayer sample.

The *M* vs *H* plots are shown in Figure 4 for **FeNi-bi** in both orientations. The magnetic behavior is anisotropic in both the remnant magnetization and coercive fields, with $H_c = 75 \pm 5$ G in the parallel orientation and $H_c = 55 \pm 5$ G when perpendicular. The coercive fields for the **FeNi-bi** are significantly smaller than those observed in the multilayer film.

The field-cooled and zero-field-cooled magnetization plots as a function of temperature for the **FeNi-mono** sample are shown in Figure 5. The magnetic response in the monolayer film shows a higher anisotropy than the bilayer or multilayer films, with the magnetization in the parallel orientation an order of magnitude more intense than the perpendicular. The parallel M_{FC} increases abruptly with decreasing temperature below $T \approx 7$ K, suggesting the onset of ferromagnetic order. The onset temperature is below the 10 K seen in the **FeNi-bi** and **FeNi-150** samples, perhaps reflecting the decrease in the number of possible exchange pathways in the isolated monolayer film.

The *M* vs *H* hysteresis loop for the **FeNi-mono** sample measured in the parallel orientation at $T = 2$ K is shown if Figure 6. The data indicate a very weak hysteresis with a coercive field on the order of $H_c = 10$ G. This value is close to the instrumental resolution, which is limited by the pinned flux within the instrument, also found to be on the order of 10 G.

Ac Magnetometry. The low-temperature magnetic behavior of the films was further probed using ac magnetometry. The temperature-dependent χ_{ac} values for **FeNi-150** in the parallel orientation, measured at 17 Hz, 170 Hz, and 1.0 kHz, are shown in Figure 7. The data show both χ' (real) and χ'' (imaginary) components. The presence of a χ'' component is indicative of uncompensated moments, and the frequency dependence of the peak position in both components is a signature of spin-glass-like behavior. The transition temperature, $T_g = 5.4$ K, is defined by the maximum in the $\chi'(T)$ plot at low frequency, here 17 Hz. The anisotropy of the magnetization is again revealed by comparing the data of Figure 7 to the $\chi_{ac}(T)$ data taken on **FeNi-150** in the

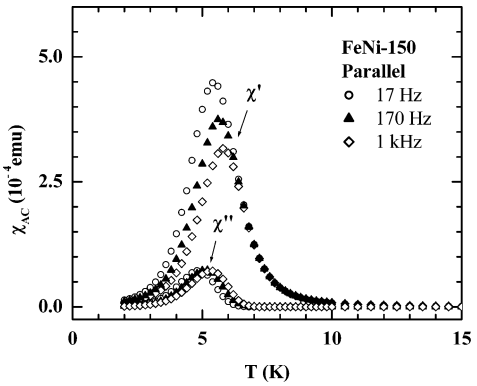

Figure 7. Background-corrected ac susceptibility, $\chi'(T)$ and $\chi''(T)$, for **FeNi-150** aligned parallel to the applied field. The samples were measured at different frequencies with an ac field of 4 G under zero-applied dc field.

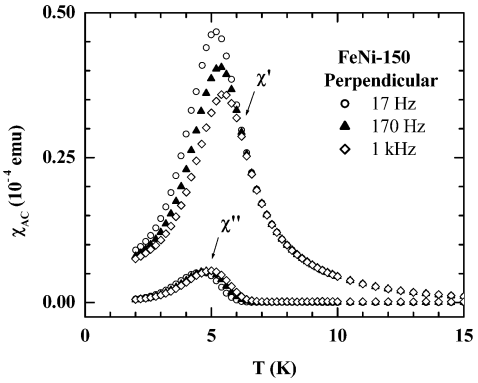

Figure 8. Background-corrected ac susceptibility, $\chi'(T)$ and $\chi''(T)$, for **FeNi-150** aligned perpendicular to the measuring field. The samples were measured at different frequencies with an ac field of 4 G under zero-applied dc field.

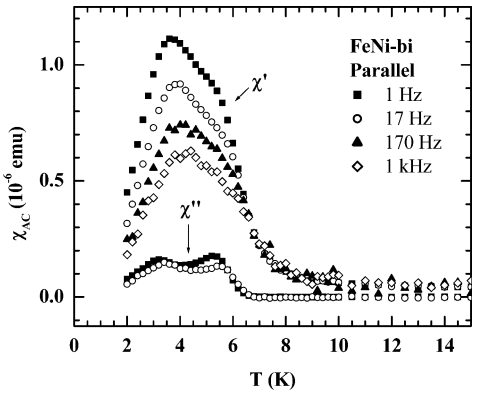

Figure 9. Background-corrected ac susceptibility, $\chi'(T)$ and $\chi''(T)$, for **FeNi-bi** aligned parallel to the measuring field. The samples were measured at different frequencies with an ac field of 4 G under zero-applied dc field.

perpendicular orientation shown in Figure 8. While the two components are present with similar frequency dependence, the magnetic response is 1 order of magnitude lower than in the parallel orientation. The temperature of the χ' maximum (5.2 K) is slightly less than that extracted from the parallel orientation.

The $\chi_{ac}(T)$ data for the parallel orientation of **FeNi-bi**, shown in Figure 9, are noticeably different than what is observed for the multilayer film. The broad feature in the $\chi'(T)$ is clearly resolved into two components in the $\chi''(T)$ data. The presence of a $\chi''(T)$ response is evidence of

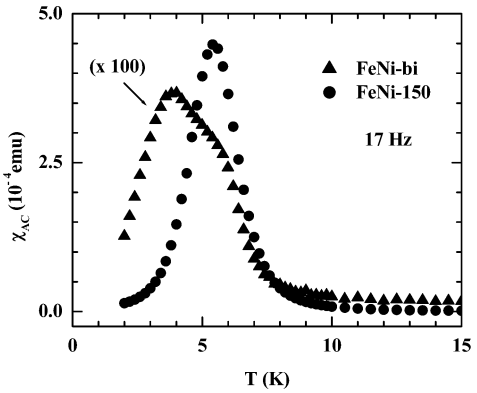

Figure 10. Background-corrected ac susceptibility, $\chi'(T)$, measured at 17 Hz for **FeNi-bi** (▲) (scaled ×100) and **FeNi-150** (●). Both samples were aligned parallel to the measuring field. The samples were measured with an ac field of 4 G under zero-applied dc field.

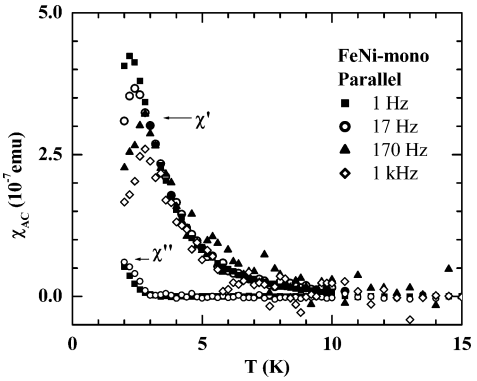

Figure 11. Background-corrected ac susceptibility, $\chi'(T)$ and $\chi''(T)$, for **FeNi-mono** aligned parallel to the measuring field. The samples were measured at different frequencies with an ac field of 4 G under zero-applied dc field.

uncompensated moments, and spin-glass-like behavior in **FeNi-bi** is also indicated by the frequency dependence of the $\chi'(T)$ and $\chi''(T)$ peak positions. The peak position of the higher temperature shoulder in $\chi'(T)$ is difficult to discern unambiguously but is very similar in position to the peak at $T_g = 5.4$ K observed for the **FeNi-150** sample at the same frequency (17 Hz). The data for the two samples are compared in Figure 10. The lower temperature peak of **FeNi-bi** yields a separate freezing temperature at 17 Hz of $T_g = 3.8$ K. An interpretation of this feature will be discussed in the next section. The anisotropy observed in the dc measurements is reproduced in the $\chi_{ac}(T)$, where the perpendicular susceptibility (not shown) is 1 order of magnitude less intense than that seen in the parallel orientation.

The $\chi_{ac}(T)$ data, measured at 1 Hz, 17 Hz, 170 Hz, and 1.0 kHz, for the parallel orientation of **FeNi-mono** are shown in Figure 11. The presence of a $\chi''(T)$ component indicates uncompensated moments in the monolayer film, albeit the peak has not clearly formed by $T = 2$ K. The effect of frequency on the $\chi''(T)$ peak position cannot be unambiguously determined; however, a shift in the onset temperature is suggested in the data. The $\chi'(T)$ clearly shows a frequency dependence, which again is indicative of spin-glass-like behavior. The glass temperature $T_g = 2.4$ K extracted from the peak position at 17 Hz is below the glass temperatures of the bilayer and multilayer films. Comparing the magnetic

response of the film in two orientations shows a magnetic anisotropy similar to that observed in the χ_{dc} measurements with χ_{AC} 1 order of magnitude larger in the parallel orientation than in the perpendicular orientation (not shown).

Discussion

Magnetic Anisotropy. The magnetic anisotropy of the thin-film samples containing the Fe−CN−Ni grid networks provides convincing evidence for the low-dimensional nature of the materials. Even though a single-crystal-like analysis is not possible, some general conclusions can be made regarding the nature of the anisotropy. The magnetic easy axis clearly has a major component oriented parallel to the plane of the substrate surface, i.e., within the plane of the grid network. This anisotropy most likely arises from the coupling of the magnetic moments to the structural anisotropy. The most pronounced anisotropic behavior is observed in the monolayer sample, **FeNi-mono**, which at $T = 2$ K has a ratio of field-cooled $M_{\parallel}$:$M_{\perp}$ of ca. 22:1. This ratio decreases in the bilayer and 150-bilayer samples to ca. 4.6:1 and 3.4:1, respectively. This trend suggests the presence of coupling between the face-to-face networks within the bilayer region. This increase in the number of exchange pathways is also evidenced by the $M_{FC}(T)$ data for the three films, shown in Figures 1, 3, and 5 where the onset of magnetization occurs at a higher temperature in the bilayer and multilayer films than in the monolayer film.

The nature of the bonding between adjacent networks within a bilayer remains uncertain. However, a comparison of the magnetic behavior of the bilayer and multilayer samples to those of other 2D metal cyanide systems provides some insight. Of particular relevance are the quasi-2D square-grid[17−20] networks constructed from iron(III) hexacyanide and nickel bis(diamine) complexes and the honeycomb[21−25] networks constructed from chromium(III) hexacyanide and nickel cyclam complexes. In general, these lamellar solids consist of cyanide-bridged two-dimensional sheets separated one from another by a solvent or counterion layer. The exchange within the sheets is ferromagnetic, but when the intersheet separation is reduced below ca. 10 Å, intersheet antiferromagnetic exchange often results in an antiferromagnetic ground state.[19,23−25,28−30] Even though the internetwork distance within the bilayers of **FeNi-150** is less than 10 Å as evidenced from X-ray diffraction data,[37] no metamagnetic behavior is observed at $T = 2$ K in the $M(H)$ data in fields up to 30 T.[38] This fact suggests that the interaction between face-to-face networks within the bilayers is predominantly covalent in nature, brought about through bridging of the axial cyanide of the amphiphilic pentacyanoferrate complex to available coordination sites on nickel ions in the adjacent network. This covalent bonding arrangement would favor ferromagnetic exchange by the same mechanism that promotes ferromagnetism within one network plane.

Spin-Glass-like Behavior. The dc magnetometry studies on each of the three samples yielded M_{ZFC} and M_{FC} traces (Figures 1, 3, and 5) with a characteristic "λ" shape that is typically observed in either ferromagnetic or spin-glass materials.[39,40] The films also displayed a hysteresis in their magnetization vs field plots that also are signs of ferromagnetic order or spin-glass-like behavior. On the other hand, the frequency dependence of the $\chi_{AC}(T)$ data for each of the three samples indicates that these materials are not long-range ordered ferromagnets at low temperature, since such systems would not show a frequency dependence in their susceptibility at or below 1 kHz. Such frequency dependence is typically assigned to either superparamagnets or spin-glasses. A spin-glass state can be distinguished from a superparamagnet by quantifying the frequency dependence through the ratio ϕ, which may be written as

$$\phi = \Delta T_f/[T_f \Delta(\log \omega)] \quad (1)$$

where T_f is the temperature at which the maximum in $\chi'(T)$ occurs, ΔT_f is the difference in T_f between an initial frequency ω and final frequency ω_f, and $\Delta(\log \omega)$ is the difference between the log of the initial and final measuring frequencies. The values of ϕ obtained for **FeNi-bi** and **FeNi-150** are 0.05 and 0.04, respectively, which fall within the range typical for insulating spin-glasses[40] and are very similar to those reported by Buschmann[35,36] and co-workers for a series of hexacyanomanganate Prussian blue analogues.

A somewhat larger value of $\phi = 0.10$ was obtained for **FeNi-mono**, which falls between the extreme cases of $\phi = 0.28$ reported for the superparamagnet α-$(Ho_2O_3)(B_2O_3)$ and $\phi \approx 0.005$ for insulating spin-glasses.[40] Fitting the data to the Arrhenius equation,

$$\ln(\tau/\tau_0) = [E_a/(k_B T)] \quad (2)$$

where τ is the average relaxation time corresponding to the frequency of the ac measurement and E_a/k_B is the energy barrier to magnetic reversal in an isolated particle, yields $1 \times 10^{-15} < \tau_0 < 1 \times 10^{-13}$ s and $E_a/k_B = 70 \pm 5$ K. This value of τ_0 is below the range of $1 \times 10^{-11} < \tau_0 < 1 \times 10^{-9}$ s predicted for noninteracting ferromagnetic particles and indicates the presence of interparticle interactions.[41] The strength of the interaction increases significantly as one progresses to the isolated bilayer and multilayer film where $1 \times 10^{-19} < \tau_0 < 1 \times 10^{-21}$ s ($E_a/k_B = 170 \pm 10$ K) and $1 \times 10^{-29} < \tau_0 < 1 \times 10^{-31}$ s ($E_a/k_B = 350 \pm 5$ K), respectively. Therefore, the system may best be described as a progression from moderately interacting ferromagnetic domains in the monolayer to a more strongly interacting glasslike state, or cluster glass, in the bilayer and multilayer films.

The two-peak profile observed in the $\chi_{ac}(T)$ data for **FeNi-bi** is unique to the single bilayer sample and warrants further discussion. Similar dual peak profiles observed in M[Mn-$(CN)_6$] (M = Cr, Mn) Prussian blue analogues have been

(38) Park, J.-H.; Culp, J. T.; Hall, D. W.; Talham, D. R.; Meisel, M. W. *Physica B*, in press.

(39) Mathieu, R.; Jonsson, P.; Nam, D. N. H.; Nordblad, P. *Phys. Rev. B* **2001**, *63*, 092401.

(40) Mydosh, J. A. *Spin Glasses*; Taylor and Francis: Washington, DC, 1993.

(41) Dormann, J. L.; Fiorani, D.; Tronc, E. In *Adv. Chem. Phys.* **1997**, *98*, 283−494.

assigned to reentrant spin-glass behavior;[36] however, such a characterization here is inappropriate since both peaks possess a frequency dependence. Therefore, neither peak corresponds to an ordered ferromagnetic state. A more likely explanation arises by comparing the $\chi_{ac}(T)$ data for **FeNi-bi** to the $\chi_{ac}(T)$ data for **FeNi-150**, as shown in Figure 10. The glass temperature is a function of disorder in a material, with more disordered phases giving lower glass transition temperatures. Analysis by grazing incidence X-ray diffraction indicates in-plane structural coherence lengths of about 6 unit cells. This estimate is an average, and each bilayer will have some domains that are larger and some smaller and some areas that are relatively disordered. The two processes observed in $\chi_{AC}(T)$ likely reflect two different sets of domains. Since the bilayers are fabricated using the same process for each sample, the **FeNi-bi** and **FeNi-150** samples should possess essentially the same degree of structural disorder within each bilayer. Therefore, the absence of a low-temperature peak in the **FeNi-150** sample may be due to interactions that are present in the multilayer sample but are absent in the single bilayer, such as long-distance dipolar exchange forces. The dipolar exchange between layers could provide an extra interaction pathway that ties the less coherent two-dimensional domains to the larger ones. The lack of similar dipolar forces in the isolated bilayer sample results in each of these sets of domains adopting a unique glass transition temperature. Similar dipolar forces have been shown to operate over relatively long distances ($\approx$35 Å inter-bilayer spacing) in other lamellar ferromagnetic materials.[42]

To influence the low-temperature magnetic response, the interlayer interaction must be on the order of about 1 K/k_B, which over the interlayer spacing of 35 Å requires moments of approximately 130 μ_B. Interestingly, the structural coherence length, estimated by grazing incidence X-ray diffraction studies,[37] corresponds to about 72 pairs of ferromagnetically coupled Fe^{3+} $S = 1/2$ and Ni^{2+} $S = 1$ ions, which can easily achieve the required moment, making this argument plausible.

(42) Laget, V.; Hornick, C.; Rabu, P.; Drillon, M.; Ziessel, R. *Coord. Chem. Rev.* **1998**, *180*, 1533−1553.

Conclusions

The interfacial assembly of a two-dimensional Fe−CN−Ni grid network in combination with the controlled deposition capability of the Langmuir−Blodgett technique yields novel low-dimensional thin films where the affects of interlayer interactions on magnetic properties can systematically be studied. Each system shows the presence of ferromagnetic domains at low temperature; however, a significant variation in magnetic behavior results upon progressing from a two-dimensional monolayer that behaves as a system of moderately interacting ferromagnetic particles to the bilayer and multilayer films that display magnetic properties of a collective glasslike state. The spin-glass behavior of the bilayer and multilayer samples likely results from spin frustration arising from a combination of structural disorder, competing exchange anisotropies between the in-plane and interplanar coupling, and the presence of dilute diamagnetic Fe(II) impurities. All of the materials studied show highly anisotropic magnetic behavior, with the highest anisotropy observed in the single-monolayer film. These progressive changes demonstrate the influences of dimensionality and interlayer coupling on the magnetic behavior in molecule-based materials.

Acknowledgment. This research was supported by the National Science Foundation through Grant DMR-9900855 (D.R.T.) and by the American Chemical Society through Grant ACS-PRF-36163-AC5 (M.W.M., D.R.T.). The authors thank Isa Benitez for her contributions to the cover artwork.

IC026158X